A Control Barrier Function Approach to Human-multi-robot Safe Interaction

Martina Lippi Alessandro Marino, *IEEE Senior Member*

***Abstract*— A fundamental prerequisite to achieve a successful human-robot cooperation is human safety, which becomes even more crucial when multiple robots are involved in the cooperative task. A general solution for addressing safety in human-multi-robot scenarios is proposed in this paper. Human safety is assessed by a safety field which accounts for the multi-robot system as a whole. The assessment of human safety is exploited within an optimization protocol where the robots' cooperative task trajectory is scaled whenever required, while exploiting the system redundancy. Control Barrier Functions (CBFs) are adopted to set up the optimization problem and kinematic and dynamic constraints are taken into consideration. Finally, simulations on a realistic setup composed of three industrial mobile manipulators show the effectiveness of the proposed solution.**

I. Introduction

bot systems and human-robot interaction represent two key topics in the current scientific scenario. The former provide enhancement of physical capabilities, execution time, and robustness of the robotic system compared to the single robot case; the latter enables benefiting from human cognitive and manipulation skills in robotic settings [1]. Merging these two components in a single system thus represents a promising direction to achieve flexible and efficient production systems handling dynamic tasks with any physical effort requirement.

However, enabling human-multi-robot collaboration requires designing rigorous strategies to ensure human safety. The presence of multiple robots in the system leads to: *i)* increased risk of collision between the human and robotic components compared to the single robot case, and *ii)* possible constraints among the robots given by collaborative tasks. A *coexistence* setting is considered in which humans and robots share the same workspace but no physical contact between them must occur. Moreover, as desirable in industrial applications, we consider that the robots' planned path should not be altered by the human avoidance strategy.

In this work, motivated by the CANOPIES project[1], that aims at devising human-multi-robot interaction strategies in the framework of precision agriculture, we propose a scaling procedure for human-multi-robot safe coexistence. We first introduce a safety field which assesses the human level of safety with respect to the entire *team* of robots. We then parameterize the cooperative task with respect to a scaling parameter which allows to modulate the robots' velocity along the path without deviating from it. The scaling parameter is determined as the output of an optimization problem based on CBF formulation where also kinematics and dynamics constraints of the robots as well as possible redundancy are taken into account. This paper builds on [2] with respect to which the following main aspects are introduced: *i)* a more general formulation of the safety field is provided which makes the multi-robot system intrinsically safe when the robots are still, and *ii)* a CBF-based solution is devised for trajectory scaling which allows to include constraints on human safety as well as on possible positions, velocities, and torques of each robot.

II. Related work

Traditional approaches for human-robot coexistence scenarios rely on carrying out evasive actions to move the robot away from the human operator. For example, geometric primitives are combined with attraction and repulsion vectors in [3], while an augmented reality based on depth sensor is exploited in [4] to stop or move the robot away from the human. Human safety assessment is also exploited to drive the evasive action, as instance, in [5].

However, all the aforementioned approaches do not guarantee any preservation of the planned path which is of interest in any precision industrial task. In this regard, the work in [6] presents a collaborative work-cell prototype in which the human operator motion is monitored through both depth and laser sensors for the sake of robustness. A Model Predictive Control is formulated in [7] where the trajectory is scaled down so as to guarantee that no collision occurs with the robot end effector while kinematic redundancy is exploited to maximize the human-robot distance. A solution compliant with the ISO/TS 15066 is then proposed in [8] where a CBF formulation is employed to modulate the robot velocity according to power and force limits regulations at the robot end effector. In addition, the entire structure of the manipulator is taken into account in [9] where an optimization problem is set up to define the velocity scaling parameter. However, no human motion is taken into account in the proposed formulation. A trajectory scaling approach for Dynamical Movement Primitives is then provided in [10] where velocity constraints are taken into account to achieve a comfortable interaction for the operator.

In the context of human-*multi*-robot interaction, most of existing results address safe navigation scenarios with no manipulators and where only goal states are assigned, i.e., no desired *path* from start to goal is provided. As instance, a framework for real-time replanning in human-multi-robot settings is devised in [11] where human prediction

M. Lippi is with Roma Tre University, Via Ostiense, 159, 00154, Rome (RM), Italy, martina.lippi@uniroma3.it

A. Marino is with University of Cassino and Southern Lazio, Via G. Di Biasio 43, 03043 Cassino (FR), Italy, al.marino@unicas.it

This work was supported by Dipartimento di Eccellenza granted to DIEI Department, University of Cassino and Southern Lazio and by H2020-ICT project CANOPIES (Grant Agreement N. 101016906).

10.1109/MED51440.2021.9480187

[1] www.canopies-project.eu

is exploited to ensure human safety in a proactive manner. However, no tight cooperative tasks and no path preserving are considered. Similarly, a human-aware navigation problem for multi-robot systems is tackled in [12] where a distributed solution based on velocity obstacles is provided.

Differently from the presented works, we aim to devise a trajectory scaling approach which is suitable for collaborative multi-robot settings and in which the human motion is taken into account as well as each robotic part is considered as a possible source of danger to the human.

III. Mathematical background

This section presents the robot modeling and a task-oriented formulation for cooperative tasks along with the robot control law. Finally, the CBF framework is recalled.

A. Robot modeling

A team of $N > 1$ mobile manipulators is considered where the generic robot i has the following dynamic model:

$$\boldsymbol{M}_i(\boldsymbol{q}_i)\ddot{\boldsymbol{q}}_i + \boldsymbol{C}_i(\boldsymbol{q}_i, \dot{\boldsymbol{q}}_i)\dot{\boldsymbol{q}}_i + \boldsymbol{F}_i\dot{\boldsymbol{q}}_i + \boldsymbol{g}_i(\boldsymbol{q}_i) = \boldsymbol{\tau}_i \quad (1)$$

where $\boldsymbol{q}_i \in \mathbb{R}^{n_i}$ ($\dot{\boldsymbol{q}}_i$, $\ddot{\boldsymbol{q}}_i$) is the joint position (velocity, acceleration) vector, $\boldsymbol{\tau}_i \in \mathbb{R}^{n_i}$ is the joint torque vector, $\boldsymbol{M}_i(\boldsymbol{q}_i) \in \mathbb{R}^{n_i \times n_i}$ is the inertia matrix, $\boldsymbol{C}_i(\boldsymbol{q}_i, \dot{\boldsymbol{q}}_i) \in \mathbb{R}^{n_i \times n_i}$ is the centrifugal and Coriolis terms matrix, $\boldsymbol{F}_i \in \mathbb{R}^{n_i \times n_i}$ is the viscous friction matrix and $\boldsymbol{g}_i(\boldsymbol{q}_i) \in \mathbb{R}^{n_i}$ is the gravity vector. The end effector configuration with respect to the world frame is denoted by $\boldsymbol{x}_i = \left[\boldsymbol{p}_i^T,\, \boldsymbol{\phi}_i^T\right]^T \in \mathbb{R}^p$, with $\boldsymbol{p}_i$ and $\boldsymbol{\phi}_i$ the position and orientation components, respectively, for which it holds

$$\ddot{\boldsymbol{x}}_i = \boldsymbol{J}_i(\boldsymbol{q}_i)\ddot{\boldsymbol{q}}_i + \dot{\boldsymbol{J}}(\boldsymbol{q}_i, \dot{\boldsymbol{q}}_i)\dot{\boldsymbol{q}}_i \quad (2)$$

with $\boldsymbol{J}_i(\boldsymbol{q}_i) \in \mathbb{R}^{p \times n_i}$ the manipulator Jacobian matrix. Let n be the total number of Degrees Of Freedom (DOFs) $n = \sum_{i=1}^{N} n_i$, the following collective variables are defined

$$\begin{aligned} \boldsymbol{x} &= \left[\boldsymbol{x}_1^T, \quad \boldsymbol{x}_2^T, \quad \ldots, \quad \boldsymbol{x}_N^T\right]^T \in \mathbb{R}^{Np} \\ \boldsymbol{q} &= \left[\boldsymbol{q}_1^T, \quad \boldsymbol{q}_2^T, \quad \ldots, \quad \boldsymbol{q}_N^T\right]^T \in \mathbb{R}^{n} \\ \boldsymbol{J}(\boldsymbol{q}) &= \mathrm{diag}\{\boldsymbol{J}_1(\boldsymbol{q}_1), \ldots, \boldsymbol{J}_N(\boldsymbol{q}_N)\} \in \mathbb{R}^{Np \times n}. \end{aligned} \quad (3)$$

Moreover, we consider that position, velocity and torque constraints exist for each manipulator as in real-world settings:

$$\boldsymbol{q}_{i,m} \leq \boldsymbol{q}_i \leq \boldsymbol{q}_{i,M},\ \dot{\boldsymbol{q}}_{i,m} \leq \dot{\boldsymbol{q}}_i \leq \dot{\boldsymbol{q}}_{i,M},\ \boldsymbol{\tau}_{i,m} \leq \boldsymbol{\tau}_i \leq \boldsymbol{\tau}_{i,M} \quad (4)$$

which are component-wise and where $\boldsymbol{q}_{i,m}$ ($\dot{\boldsymbol{q}}_{i,m}$, $\boldsymbol{\tau}_{i,m}$) and $\boldsymbol{q}_{i,M}$ ($\dot{\boldsymbol{q}}_{i,M}$, $\boldsymbol{\tau}_{i,M}$) are the minimum and maximum joint position (velocity, torque) values, respectively. Torque bounds can be converted into acceleration bounds provided that an accurate model of (1) is available and by exploiting the following quantities

$$\begin{cases} \boldsymbol{\chi}_{i,1} = \boldsymbol{M}_i(\boldsymbol{q}_i)^{-1}\Big(\boldsymbol{\tau}_{i,M} - \boldsymbol{C}_i(\boldsymbol{q}_i, \dot{\boldsymbol{q}}_i)\dot{\boldsymbol{q}}_i - \boldsymbol{F}_i\dot{\boldsymbol{q}}_i - \boldsymbol{g}_i(\boldsymbol{q}_i)\Big) \\ \boldsymbol{\chi}_{i,2} = \boldsymbol{M}_i(\boldsymbol{q}_i)^{-1}\Big(\boldsymbol{\tau}_{i,m} - \boldsymbol{C}_i(\boldsymbol{q}_i, \dot{\boldsymbol{q}}_i)\dot{\boldsymbol{q}}_i - \boldsymbol{F}_i\dot{\boldsymbol{q}}_i - \boldsymbol{g}_i(\boldsymbol{q}_i)\Big) \end{cases}$$

which depend on the robot state. Let us introduce the variables $\ddot{\boldsymbol{q}}_{i,m} = \min\{\boldsymbol{\chi}_{i,1}, \boldsymbol{\chi}_{i,2}\}$ and $\ddot{\boldsymbol{q}}_{i,M} = \max\{\boldsymbol{\chi}_{i,1}, \boldsymbol{\chi}_{i,2}\}$, with $\min, \max$ intended component-wise, it follows

$$\ddot{\boldsymbol{q}}_{i,m} \leq \ddot{\boldsymbol{q}}_i \leq \ddot{\boldsymbol{q}}_{i,M}. \quad (5)$$

B. Cooperative task specification

The robot cooperative task is specified by a task function $\boldsymbol{\sigma}(\boldsymbol{x}) \in \mathbb{R}^m$ depending on the collective vector $\boldsymbol{x}$

$$\boldsymbol{\sigma} = \boldsymbol{J}_\sigma \boldsymbol{x}, \quad \dot{\boldsymbol{\sigma}} = \boldsymbol{J}_\sigma \dot{\boldsymbol{x}}, \quad \ddot{\boldsymbol{\sigma}} = \boldsymbol{J}_\sigma \ddot{\boldsymbol{x}} \quad (6)$$

with $\boldsymbol{J}_\sigma \in \mathbb{R}^{m \times Np}$ the constant task Jacobian matrix that can be used to formalize a variety of multi-robot tasks [13] (see an example in Sec. VI). A desired *nominal* trajectory $\boldsymbol{\sigma}_n(t)$ ($\dot{\boldsymbol{\sigma}}_n(t)$, $\ddot{\boldsymbol{\sigma}}_n(t)$) corresponding to the task variables in (6) is assumed to be available. The trajectory is parameterized through a parameter $c(t)$ such that $c : [t_0, t_f] \in \mathbb{R} \to [t_0, t_f] \in \mathbb{R}$, with t_0 and t_f the start and final time instants of the nominal trajectory, respectively. Based on $c(t)$, a *reference* trajectory $\boldsymbol{\sigma}_r(t)$ ($\dot{\boldsymbol{\sigma}}_r(t)$, $\ddot{\boldsymbol{\sigma}}_r(t)$) is generated:

$$\begin{cases} \boldsymbol{\sigma}_r(t) = \boldsymbol{\sigma}_n(c(t)) \\ \dot{\boldsymbol{\sigma}}_r(t) = \dfrac{\partial \boldsymbol{\sigma}_n(c(t))}{\partial c}\dot{c}(t) \\ \ddot{\boldsymbol{\sigma}}_r(t) = \dfrac{\partial^2 \boldsymbol{\sigma}_n(c(t))}{\partial c^2}\dot{c}^2(t) + \dfrac{\partial \boldsymbol{\sigma}_n(c(t))}{\partial c}\ddot{c}(t) \end{cases} \quad (7)$$

which is the trajectory actually tracked by the robots. It follows that the case $c(t) = t$ implies $\boldsymbol{\sigma}_n(c(t)) = \boldsymbol{\sigma}_n(t)$ and that $\dot{c} = 1, \ddot{c} = 0$ implies $\dot{\boldsymbol{\sigma}}_n(c(t)) = \dot{\boldsymbol{\sigma}}_n(t)$, $\ddot{\boldsymbol{\sigma}}_n(c(t)) = \ddot{\boldsymbol{\sigma}}_n(t)$. The rationale behind this design choice is that, by modulating the scaling parameter $c(t)$, the nominal trajectory $\boldsymbol{\sigma}_n(t)$ can be online scaled to take into account human safety.

C. Multi-robot low-level control

Let $\boldsymbol{q}_{r,i}(t) \in \mathbb{R}^{n_i}$ ($\dot{\boldsymbol{q}}_{r,i}(t)$, $\ddot{\boldsymbol{q}}_{r,i}(t)$) be the reference joint position (velocity, acceleration) of robot i. We make the following assumption which is typically fulfilled for off-the-shelf robots.

Assumption 1. *Each robot is equipped with an inner motion control loop which guarantees tracking of a reference joint trajectory, i.e.,* $\boldsymbol{q}_{r,i} \approx \boldsymbol{q}_i$ ($\dot{\boldsymbol{q}}_{r,i} \approx \dot{\boldsymbol{q}}_i$, $\ddot{\boldsymbol{q}}_{r,i} \approx \ddot{\boldsymbol{q}}_i$).

Based on the above assumption and on the kinematic model (2), the following virtual model is considered

$$\ddot{\boldsymbol{x}}_i = \boldsymbol{J}_i(\boldsymbol{q}_i)\boldsymbol{u}_i + \dot{\boldsymbol{J}}_i(\boldsymbol{q}_i, \dot{\boldsymbol{q}}_i)\dot{\boldsymbol{q}}_i \quad (8)$$

where $\boldsymbol{u}_i = \ddot{\boldsymbol{q}}_i \approx \ddot{\boldsymbol{q}}_{r,i}$ is the input of the assumed virtual model to design for tracking the cooperative reference trajectory $\boldsymbol{\sigma}_r(t)$. By virtue of (3), the overall system dynamics is

$$\ddot{\boldsymbol{x}} = \boldsymbol{J}(\boldsymbol{q})\boldsymbol{u} + \dot{\boldsymbol{J}}(\boldsymbol{q}, \dot{\boldsymbol{q}})\dot{\boldsymbol{q}} \quad (9)$$

with $\boldsymbol{u} = \left[\boldsymbol{u}_1^T, \ldots, \boldsymbol{u}_N^T\right]^T \in \mathbb{R}^n$. The input $\boldsymbol{u}$ is designed by resorting to a standard closed loop inverse kinematic law [14]

$$\boldsymbol{u} = \boldsymbol{J}^\dagger \left[\boldsymbol{J}_\sigma^\dagger\big(\ddot{\boldsymbol{\sigma}}_r + k_{\sigma,d}\dot{\tilde{\boldsymbol{\sigma}}} + k_{\sigma,p}\tilde{\boldsymbol{\sigma}}\big) - \dot{\boldsymbol{J}}\dot{\boldsymbol{q}}\right] + \Delta\boldsymbol{u} \quad (10)$$

where $\tilde{\boldsymbol{\sigma}}(t) = \boldsymbol{\sigma}_r(t) - \boldsymbol{\sigma}(\boldsymbol{x}(t)) \in \mathbb{R}^m$ is the task tracking error, $\Delta\boldsymbol{u} = \left[\Delta\boldsymbol{u}_1^T, \ldots, \Delta\boldsymbol{u}_N^T\right]^T \in \mathbb{R}^n$ is an additional input. By recalling (2) and (6), it easily follows:

$$\boldsymbol{J}_\sigma(\boldsymbol{J}\boldsymbol{u} + \dot{\boldsymbol{J}}\dot{\boldsymbol{q}}) = \boldsymbol{J}_\sigma\ddot{\boldsymbol{x}} = \ddot{\boldsymbol{\sigma}} = \ddot{\boldsymbol{\sigma}}_r + k_{\sigma,d}\dot{\tilde{\boldsymbol{\sigma}}} + k_{\sigma,p}\tilde{\boldsymbol{\sigma}} + \boldsymbol{J}_\sigma\boldsymbol{J}\Delta\boldsymbol{u}$$

which can be rewritten as $\ddot{\tilde{\boldsymbol{\sigma}}} + k_{\sigma,d}\dot{\tilde{\boldsymbol{\sigma}}} + k_{\sigma,p}\tilde{\boldsymbol{\sigma}} = -\boldsymbol{J}_\sigma\boldsymbol{J}\Delta\boldsymbol{u}$ according to which the error $\tilde{\boldsymbol{\sigma}}$ exponentially converges to the origin in the case $\boldsymbol{J}\Delta\boldsymbol{u} = \boldsymbol{0}$.

D. Exponential Control Barrier Function

In this section, we briefly review the theory underlying CBFs which allows to handle constraint set-based tasks [15]. Let us a consider a system with dynamics

$$\dot{\boldsymbol{\xi}} = \boldsymbol{f}(t, \boldsymbol{\xi}) + \boldsymbol{g}(\boldsymbol{\xi})\boldsymbol{u} \tag{11}$$

where $\boldsymbol{f}$ and $\boldsymbol{g}$ are Lipschitz-continuous vector fields, $\boldsymbol{\xi} \in \mathcal{D} \subset \mathbb{R}^l$ and $\boldsymbol{u} \in \mathcal{U} \subset \mathbb{R}^q$ are state and input of the system, respectively. Let the kth generic constraint be expressed in the following general form $h_k(t, \boldsymbol{\xi}) \geq 0$ where $h_k(\cdot)$ is a continuous differentiable function in the domain $\mathcal{D}$. The following sets are defined: $\mathcal{C}_k = \{\boldsymbol{\xi} \in \mathbb{R}^l : h_k(\boldsymbol{\xi}) \geq 0\}$, $\partial\mathcal{C}_k = \{\boldsymbol{\xi} \in \mathbb{R}^l : h_k(\boldsymbol{\xi}) = 0\}$ and $\text{Int}(\mathcal{C}_k) = \{\boldsymbol{\xi} \in \mathbb{R}^l : h_k(\boldsymbol{\xi}) > 0\}$, implying that the state $\boldsymbol{\xi}$ is required to belong to the set $\mathcal{C}_k$ in order to satisfy constraint h_k. Let us assume that the relative degree r of h_k is greater or equal to 1, i.e., $\forall \boldsymbol{\xi} \in \mathcal{D}$, $L_g L_f^i h_k(\boldsymbol{\xi}) = 0, \forall i \leq r-2$, $L_g L_f^{r-1} h_k(\boldsymbol{\xi}) \neq 0$ with $L_f h_k$, $L_g h_k$ the Lie derivatives of h_k with respect to $\boldsymbol{f}$ and $\boldsymbol{g}$, respectively, and let us define vector $\boldsymbol{\eta}(\boldsymbol{\xi}) = [h_k \; L_f h_k \; \cdots \; L_f^{r-1} h_k]$, then h_k is an Exponential CBF for (13) if there exists a vector $\boldsymbol{K}_\eta \in \mathbb{R}^{1\times r}$ such that

$$\sup_{\boldsymbol{u}\in\mathcal{U}} \left[L_f^r h_k(\boldsymbol{\xi}) + L_g L_f^{r-1} h_k(\boldsymbol{\xi})\boldsymbol{u} \right] \geq -\boldsymbol{K}_\eta \boldsymbol{\eta}(\boldsymbol{\xi}) \tag{12}$$

with $-\boldsymbol{K}_\eta$ coefficients of a Hurwitz polynomial, and the set $\mathcal{C}_k$ is positively forward invariant. Since (12) is affine in the control input $\boldsymbol{u}$, the latter can be computed as the result of a convex optimization problem subject to constraint (12)

$$\begin{aligned} \boldsymbol{u}^\star = &\arg\min_{\boldsymbol{u}} \frac{1}{2} \left(\boldsymbol{u} - \boldsymbol{u}_{(\cdot)}\right)^T \boldsymbol{Q} \left(\boldsymbol{u} - \boldsymbol{u}_{(\cdot)}\right) \\ s.t. \quad &\sup_{\boldsymbol{u}\in\mathcal{U}} \left[L_f^r h_k(\boldsymbol{\xi}) + L_g L_f^{r-1} h_k(\boldsymbol{\xi})\boldsymbol{u} \right] \geq -\boldsymbol{K}_\eta \boldsymbol{\eta}(\boldsymbol{\xi}), \quad \forall\, k \end{aligned} \tag{13}$$

where $\boldsymbol{u}_{(\cdot)}$ is the desired nominal input as specified in the following and $\boldsymbol{Q} \in \mathbb{R}^{q\times q}$ is a positive definite matrix.

IV. Human safety assessment

Building on [2], a safety field accounting for human-multi-robot relative position and velocity is defined. The following features are embedded:

- F.1 the case of still robots is intrinsically safe having the field not falling below a provided minimum value;
- F.2 the lower the human-robot relative distance, the lower the safety;
- F.3 when robots and human are moving against each other, safety must decrease depending on the negative relative velocity, while when they are moving away from each other, safety must increase depending on positive relative velocity.

The case of single point P of the robot structure and single point P_o of the human operator is first considered and the following local scalar safety index is defined:

$$f(\boldsymbol{p}, \dot{\boldsymbol{p}}, \boldsymbol{p}_o, \dot{\boldsymbol{p}}_o) = \alpha_1(d) + m(\dot{\boldsymbol{p}})\alpha_2(d, \dot{d}) + (1 - m(\dot{\boldsymbol{p}}))f_{min} \tag{14}$$

where $\boldsymbol{p}\,(\dot{\boldsymbol{p}}) \in \mathbb{R}^3$ is the position (velocity) vector of the robot point P, $\boldsymbol{p}_o\,(\dot{\boldsymbol{p}}_o) \in \mathbb{R}^3$ is the position (velocity) vector of the human point P_o, $d = \|\boldsymbol{p} - \boldsymbol{p}_o\|$ is the distance between P and P_o, $m(\dot{\boldsymbol{p}})$ is a smooth modulating function which is monotonically increasing with respect to $\|\dot{\boldsymbol{p}}\|$ and is 0 for $\|\dot{\boldsymbol{p}}\| = 0$ (still robot point P), and 1 for $\|\dot{\boldsymbol{p}}\| \geq m_h$ (moving robot point P), with $m_h \in \mathbb{R}^+$ a threshold to design and, finally, f_{min} is the local minimum safety, which is always fulfilled when $\|\dot{\boldsymbol{p}}\| = 0$. Note that the modulating function m allows to guarantee feature F.1. Moreover, the higher the threshold m_h, the larger the range of velocities in which the the robot is considered safe. Such a feature can be adopted to account, for example, for the size of the robot (greater for small-size robots and lower for medium or big ones).
Concerning function α_1, it is any non negative continuous monotonically increasing Lipschitz function accounting for F.2. Function $\alpha_2(d, \dot{d})$ is any continuous monotonically increasing function with respect to $\dot{d}$ which is negative for $\dot{d} < 0$ and positive for $\dot{d} > 0$; then, according to F.3, it decreases the value of the field f whenever the relative distance is decreasing and increases f when the relative distance is increasing. A possible choice of α_1, α_2 and m in (14) is:

$$\begin{cases} \alpha_1(d) = d, \qquad \alpha_2(d) = \tanh(\dot{d}) \\ m(\dot{\boldsymbol{p}}) = \begin{cases} 6\left(\frac{\|\dot{p}\|}{m_h}\right)^5 - 15\left(\frac{\|\dot{p}\|}{m_h}\right)^4 + 10\left(\frac{\|\dot{p}\|}{m_h}\right)^3, & \frac{\|\dot{p}\|}{m_h} \leq 1 \\ 0, & \frac{\|\dot{p}\|}{m_h} > 1. \end{cases} \end{cases} \tag{15}$$

We can now introduce the global safety field associated with the human-multi-robot system. As in [16], the end points of the links of the human skeleton are considered. The cumulative safety index related to robot i is obtained by integrating f in (14) along the robot links and by evaluating it for each human point [2]. Each link l of robot i is modeled as a segment starting at $\boldsymbol{p}_{i,l}^0$ and ending at $\boldsymbol{p}_{i,l}^1$:

$$\begin{cases} F_{i,l} = \displaystyle\int_0^1 f(\boldsymbol{p}_{i,l}^s, \dot{\boldsymbol{p}}_{i,l}^s, \boldsymbol{p}_o, \dot{\boldsymbol{p}}_o) ds \\ \boldsymbol{p}_{i,l}^s = \boldsymbol{p}_{i,l}^0 + (\boldsymbol{p}_{i,l}^1 - \boldsymbol{p}_{i,l}^0)s \\ \dot{\boldsymbol{p}}_{i,l}^s = \dot{\boldsymbol{p}}_{i,l}^0 + (\dot{\boldsymbol{p}}_{i,l}^1 - \dot{\boldsymbol{p}}_{i,l}^0)s \end{cases} \tag{16}$$

with $s \in [0, 1]$. By denoting with n_o the total number of human points and with $\boldsymbol{p}_{o,j}$ the position of the jth one, the safety index associated with the jth human point with respect to the ith robot can be easily defined from (16) as

$$\bar{F}_{i,j} = \textstyle\sum_{l=1}^{n_i} F_{i,l}(\boldsymbol{p}_{i,l}^0, \boldsymbol{p}_{i,l}^1, \dot{\boldsymbol{p}}_{i,l}^0, \dot{\boldsymbol{p}}_{i,l}^1, \boldsymbol{p}_{o,j}, \dot{\boldsymbol{p}}_{o,j}). \tag{17}$$

By considering all the human points, the cumulative safety index associated with the ith robot can be derived

$$\bar{F}_i = \frac{1}{n_o} \textstyle\sum_{j=1}^{n_o} \bar{F}_{i,j}(\boldsymbol{q}_i, \dot{\boldsymbol{q}}_i, \boldsymbol{p}_{o,j}, \dot{\boldsymbol{p}}_{o,j}) \tag{18}$$

which is finally extended to the team of robots as follows

$$\bar{F} = \textstyle\sum_{i=1}^{N} \bar{F}_i, \quad \dot{\bar{F}} = \sum_{i=1}^{N} \dot{\bar{F}}_i. \tag{19}$$

V. Problem statement and proposed solution

In this section, the main problem addressed in the paper is formulated, and the derivative of the safety field is computed. The latter is finally exploited to define a CBF-based solution.

Problem 1. *Let us consider N mobile manipulators performing a cooperative task expressed by a task function $\boldsymbol{\sigma}(\boldsymbol{x})$ in* (6)*, for which a desired trajectory $\boldsymbol{\sigma}_n(t)$ is assigned. Let us consider a human operator shares the same workspace of the robots and the level of human safety is assessed by the index $\bar{F}(t)$ in* (19)*, for which a time-varying minimum value $\bar{F}_{min}(t)$ is assigned. The objective is to modify $\boldsymbol{\sigma}_n(t)$ to generate a reference trajectory $\boldsymbol{\sigma}_r(t)$ in* (7) *which guarantees the safety condition $\bar{F}(t) \geq \bar{F}_{min}(t)$, $\forall t$, to be always satisfied while meeting the robots position, velocity and acceleration constraints in* (5)*.*

In [2], it is proven that $\bar{F}_{min}(t)$ can be chosen in such a way to ensure a minimum safety distance between the human operator and any robots in the team. A further possibility consists in experimentally calibrating $\bar{F}_{min}$ according to the estimated human stress or perceived level of danger [17].

A. Time derivative of the safety field $\bar{F}$

In the following, the time derivative of the safety field $\bar{F}$ in (19) is computed. To this aim, the derivative of *local* safety field f in (14) is first computed:

$$\dot{f} = \left(\frac{\partial \alpha_1(d^s_{i,l})}{\partial d^s_{i,l}} + m(\dot{\boldsymbol{p}}^s_{i,l}) \frac{\partial \alpha_2(d^s_{i,l}, \dot{d}^s_{i,l})}{\partial d^s_{i,l}} \right) \dot{d}^s_{i,l} + m(\dot{\boldsymbol{p}}^s_{i,l}) \frac{\partial \alpha_2(d^s_{i,l}, \dot{d}^s_{i,l})}{\partial \dot{d}^s_{i,l}} \ddot{d}^s_{i,l} + \left(\alpha_2(d^s_{i,l}, \dot{d}^s_{i,l}) - f_{min} \right) \frac{\partial m(\dot{\boldsymbol{p}}^s_{i,l})}{\partial \dot{\boldsymbol{p}}^s_{i,l}}^T \ddot{\boldsymbol{p}}^s_{i,l} \tag{20}$$

where $d^s_{i,l} = \|\boldsymbol{p}^s_{i,l} - \boldsymbol{p}_o\|$. Note that whenever the robot point is still ($\dot{\boldsymbol{p}}^s_{i,l} = \boldsymbol{0}_p$), being $\partial m(\dot{\boldsymbol{p}}^s_{i,l})/\partial \dot{\boldsymbol{p}}^s_{i,l} = \boldsymbol{0}_p^T$ and $m(\dot{\boldsymbol{p}}^s_{i,l}) = 0$, it holds $\dot{f} = \partial \alpha_1(d^s_{i,l})/\partial d^s_{i,l}$, which means that the safety field can only change if the human moves in such a way to modify the distance $d^s_{i,l}$.

By differentiating the distance term, one obtains

$$\dot{d}^s_{i,l} = \frac{(\boldsymbol{p}^s_{i,l} - \boldsymbol{p}_o)^T (\dot{\boldsymbol{p}}^s_{i,l} - \dot{\boldsymbol{p}}_o)}{d^s_{i,l}}, \quad \ddot{d}^s_{i,l} = \boldsymbol{\beta}_1^T \ddot{\boldsymbol{p}}^s_{i,l} + \beta_2$$

with $d^s_{i,l} \neq 0$ and $\boldsymbol{\beta}_1 \in \mathbb{R}^3$ and $\boldsymbol{\beta}_2 \in \mathbb{R}$ defined as

$$\begin{cases} \boldsymbol{\beta}_1 = \dfrac{\boldsymbol{p}^s_{i,l} - \boldsymbol{p}_o}{d^s_{i,l}} \\ \beta_2 = -\boldsymbol{\beta}_1^T \ddot{\boldsymbol{p}}_o + \dfrac{\|\dot{\boldsymbol{p}}^s_{i,l} - \dot{\boldsymbol{p}}_o\|^2}{d^s_{i,l}} - \dfrac{[\boldsymbol{\beta}_1^T (\dot{\boldsymbol{p}}^s_{i,l} - \dot{\boldsymbol{p}}_o)]^2}{d^s_{i,l}}. \end{cases}$$

Now, let us consider the relation between the linear acceleration $\ddot{\boldsymbol{p}}^s_{i,l}$ and the joints variables of the same robot i, i.e.,

$$\ddot{\boldsymbol{p}}^s_{i,l} = \boldsymbol{J}^s_{i,l}(\boldsymbol{q}_i) \ddot{\boldsymbol{q}}_i + \dot{\boldsymbol{J}}^s_{i,l}(\boldsymbol{q}_i, \dot{\boldsymbol{q}}_i) \dot{\boldsymbol{q}}_i \tag{21}$$

with $\boldsymbol{J}^s_{i,l} \in \mathbb{R}^{3 \times n_i}$ the positional Jacobian matrix associated with $\boldsymbol{p}^s_{i,l}$. Considering (10), (21) can be rewritten as

$$\ddot{\boldsymbol{p}}^s_{i,l} = \boldsymbol{J}^s_{i,l} \boldsymbol{S}_i \boldsymbol{J}^\dagger \left[\boldsymbol{J}^\dagger_\sigma (\ddot{\boldsymbol{\sigma}}_r + k_{\sigma,d} \dot{\tilde{\boldsymbol{\sigma}}} + k_{\sigma,p} \tilde{\boldsymbol{\sigma}}) - \dot{\boldsymbol{J}} \dot{\boldsymbol{q}} \right] + \boldsymbol{J}^s_{i,l} \Delta \boldsymbol{u}_i + \dot{\boldsymbol{J}}^s_{i,l} \dot{\boldsymbol{q}}_i \tag{22}$$

where $\boldsymbol{S}_i \in \mathbb{R}^{n_i \times n}$ is a selection matrix defined as

$$\boldsymbol{S}_i = \{ \boldsymbol{O}_{n_1} \quad \cdots \quad \underbrace{\boldsymbol{I}_{n_i}}_{i \text{ th robot}} \quad \cdots \quad \boldsymbol{O}_{n_N} \}. \tag{23}$$

By considering the reference trajectory in (7), (22) leads to

$$\ddot{\boldsymbol{p}}^s_{i,l} = \boldsymbol{\gamma}_1 \ddot{c} + \boldsymbol{\Gamma}_2 \Delta \boldsymbol{u}_i + \boldsymbol{\gamma}_3 \tag{24}$$

that is linear with respect to $\ddot{c}$ and $\Delta \boldsymbol{u}_i$ and where the coefficients $\boldsymbol{\gamma}_1, \boldsymbol{\gamma}_3 \in \mathbb{R}^3$ and $\boldsymbol{\Gamma}_2 \in \mathbb{R}^{3 \times n_i}$ are defined as:

$$\begin{cases} \boldsymbol{\gamma}_1 = \boldsymbol{J}^s_{i,l} \boldsymbol{S}_i \boldsymbol{J}^\dagger \boldsymbol{J}^\dagger_\sigma \dfrac{\partial \boldsymbol{\sigma}_n}{\partial c}, & \boldsymbol{\gamma}_2 = \boldsymbol{J}^s_{i,l} \\ \boldsymbol{\gamma}_3 = \boldsymbol{J}^s_{i,l} \boldsymbol{S}_i \boldsymbol{J}^\dagger \left[\boldsymbol{J}^\dagger_\sigma \left(\dfrac{\partial^2 \boldsymbol{\sigma}_n}{\partial c^2} \dot{c}^2 + k_{\sigma,d} \dot{\tilde{\boldsymbol{\sigma}}} + k_{\sigma,p} \tilde{\boldsymbol{\sigma}} \right) - \dot{\boldsymbol{J}} \dot{\boldsymbol{q}} \right] + \dot{\boldsymbol{J}}^s_{i,l} \dot{\boldsymbol{q}}_i. \end{cases}$$

In view of (20) and (24), it follows $\dot{f} = \lambda_1 \ddot{c} + \boldsymbol{\lambda}_2^T \Delta \boldsymbol{u}_i + \lambda_3$ where the expressions of λ_1, $\lambda_3 \in \mathbb{R}$ and $\boldsymbol{\lambda}_2 \in \mathbb{R}^3$ are

$$\begin{cases} \lambda_1 = m(\dot{\boldsymbol{p}}^s_{i,l}) \boldsymbol{\beta}_1^T \boldsymbol{\gamma}_1 \dfrac{\partial \alpha_2}{\partial \dot{d}^s_{i,l}} + (\alpha_2 - f_{min}) \dfrac{\partial m(\dot{\boldsymbol{p}}^s_{i,l})}{\partial \dot{\boldsymbol{p}}^s_{i,l}}^T \boldsymbol{\gamma}_1 \\ \boldsymbol{\lambda}_2^T = m(\dot{\boldsymbol{p}}^s_{i,l}) \boldsymbol{\beta}_1^T \boldsymbol{\Gamma}_2 \dfrac{\partial \alpha_2}{\partial \dot{d}^s_{i,l}} + (\alpha_2 - f_{min}) \dfrac{\partial m(\dot{\boldsymbol{p}}^s_{i,l})}{\partial \dot{\boldsymbol{p}}^s_{i,l}}^T \boldsymbol{\Gamma}_2 \\ \lambda_3 = m(\dot{\boldsymbol{p}}^s_{i,l}) (\boldsymbol{\beta}_1^T \boldsymbol{\gamma}_3 + \beta_2) \dfrac{\partial \alpha_2}{\partial \dot{d}^s_{i,l}} + \left(\dfrac{\partial \alpha_1}{\partial d^s_{i,l}} + m(\dot{\boldsymbol{p}}^s_{i,l}) \dfrac{\partial \alpha_2}{\partial d^s_{i,l}} \right) \dot{d}^s_{i,l} \\ \qquad + (\alpha_2 - f_{min}) \dfrac{\partial m(\dot{\boldsymbol{p}}^s_{i,l})}{\partial \dot{\boldsymbol{p}}^s_{i,l}}^T \boldsymbol{\gamma}_3. \end{cases}$$

Therefore, by virtue of (16), (17) and (18), $\dot{f}$ is extended to the entire structure of the i th manipulator:

$$\dot{\bar{F}}_i = \mu_{1,i} \ddot{c} + \boldsymbol{\mu}^T_{2,i} \Delta \boldsymbol{u}_i + \mu_{3,i}$$

with $\mu_{1,i}, \mu_{3,i} \in \mathbb{R}$ and $\boldsymbol{\mu}_{2,i} \in \mathbb{R}^3$ defined as

$$\begin{cases} \mu_{1,i} = \dfrac{1}{n_o} \displaystyle\sum_{j=1}^{n_o} \sum_{l=1}^{n_i} \int_0^1 \lambda_1(\boldsymbol{p}^s_{i,l}, \dot{\boldsymbol{p}}^s_{i,l}, \boldsymbol{p}_{o,j}, \dot{\boldsymbol{p}}_{o,j}, \boldsymbol{q}_i, \dot{\boldsymbol{q}}_i, c)\, ds \\ \boldsymbol{\mu}^T_{2,i} = \dfrac{1}{n_o} \displaystyle\sum_{j=1}^{n_o} \sum_{l=1}^{n_i} \int_0^1 \lambda_2(\boldsymbol{p}^s_{i,l}, \dot{\boldsymbol{p}}^s_{i,l}, \boldsymbol{p}_{o,j}, \dot{\boldsymbol{p}}_{o,j}, \ddot{\boldsymbol{p}}_{o,j}, \boldsymbol{q}_i, \dot{\boldsymbol{q}}_i, c, \dot{c})\, ds \\ \mu_{3,i} = \dfrac{1}{n_o} \displaystyle\sum_{j=1}^{n_o} \sum_{l=1}^{n_i} \int_0^1 \lambda_3(\boldsymbol{p}^s_{i,l}, \dot{\boldsymbol{p}}^s_{i,l}, \boldsymbol{p}_{o,j}, \dot{\boldsymbol{p}}_{o,j}, \ddot{\boldsymbol{p}}_{o,j}, \boldsymbol{q}_i, \dot{\boldsymbol{q}}_i, c, \dot{c})\, ds. \end{cases}$$

Finally, the time derivative of $\bar{F}(t)$ in (19) is expressed as

$$\dot{\bar{F}}(t) = \mu_1(t)\, \ddot{c}(t) + \boldsymbol{\mu}_2(t)^T \Delta \boldsymbol{u} + \mu_3(t) \tag{25}$$

with $\mu_1 = \sum_{i=1}^N \mu_{1,i}$, $\boldsymbol{\mu}_2 = [\boldsymbol{\mu}^T_{1,i} \ \ldots \ \boldsymbol{\mu}^T_{N,i}]^T \in \mathbb{R}^n$ and $\mu_3 = \sum_{i=1}^N \mu_{3,i}$.

B. Proposed solution

We are now ready to present the proposed solution to Problem 1. Let us consider the model in (9) that implies $\ddot{\boldsymbol{q}} = \boldsymbol{u}$. The latter can be rewritten as

$$\begin{bmatrix} \dot{\boldsymbol{q}} \\ \ddot{\boldsymbol{q}} \end{bmatrix} = \begin{bmatrix} \boldsymbol{O}_n & \boldsymbol{I}_n \\ \boldsymbol{O}_n & \boldsymbol{O}_n \end{bmatrix} \begin{bmatrix} \boldsymbol{q} \\ \dot{\boldsymbol{q}} \end{bmatrix} + \begin{bmatrix} \boldsymbol{O}_n \\ \boldsymbol{I}_n \end{bmatrix} \boldsymbol{u} \tag{26}$$

which, by virtue of (7) and the control input (10), leads to

$$\begin{aligned} \begin{bmatrix} \dot{\boldsymbol{q}} \\ \ddot{\boldsymbol{q}} \end{bmatrix} &= \begin{bmatrix} \boldsymbol{O}_n & \boldsymbol{I}_n \\ \boldsymbol{O}_n & \boldsymbol{O}_n \end{bmatrix} \begin{bmatrix} \boldsymbol{q} \\ \dot{\boldsymbol{q}} \end{bmatrix} + \begin{bmatrix} \boldsymbol{O}_n & 0 \\ \boldsymbol{I}_n & \boldsymbol{J}^\dagger \boldsymbol{J}^\dagger_\sigma \frac{\partial \boldsymbol{\sigma}_n}{\partial c} \end{bmatrix} \begin{bmatrix} \Delta \boldsymbol{u} \\ \ddot{c} \end{bmatrix} \\ &\quad + \begin{bmatrix} \boldsymbol{O}_n \\ \boldsymbol{I}_n \end{bmatrix} \left(\boldsymbol{J}^\dagger \left[\boldsymbol{J}^\dagger_\sigma \left(\frac{\partial^2 \boldsymbol{\sigma}_n}{\partial c^2} \dot{c}^2(t) + k_{\sigma,d} \dot{\tilde{\boldsymbol{\sigma}}} + k_{\sigma,p} \tilde{\boldsymbol{\sigma}} \right) - \dot{\boldsymbol{J}} \dot{\boldsymbol{q}} \right] \right) \\ &= \boldsymbol{f}_q(t, \boldsymbol{q}, \dot{\boldsymbol{q}}, c, \dot{c}) + \boldsymbol{g}_q(t, \boldsymbol{q}, \dot{\boldsymbol{q}}) \begin{bmatrix} \Delta \boldsymbol{u} \\ \ddot{c} \end{bmatrix} \end{aligned}$$

where the expressions of $\boldsymbol{f}_q$ and $\boldsymbol{g}_q$ are straightforward. By setting $\ddot{c} = u_c$, it holds

$$\begin{bmatrix} \dot{c} \\ \ddot{c} \end{bmatrix} = \begin{bmatrix} 0 & 1 \\ 0 & 0 \end{bmatrix} \begin{bmatrix} c \\ \dot{c} \end{bmatrix} + \begin{bmatrix} \boldsymbol{0}_{n,1} & 0 \\ \boldsymbol{0}_{n,1} & 1 \end{bmatrix} \begin{bmatrix} \Delta \boldsymbol{u} \\ u_c \end{bmatrix} = \boldsymbol{f}_c(c, \dot{c}) + \boldsymbol{g}_c(c, \dot{c}) \begin{bmatrix} \Delta \boldsymbol{u} \\ u_c \end{bmatrix} \tag{27}$$

where, again, $\boldsymbol{f}_c$ and $\boldsymbol{g}_c$ can be easily computed. Therefore, the overall system dynamics is

$$\begin{bmatrix} \dot{\boldsymbol{q}} \\ \ddot{\boldsymbol{q}} \\ \dot{c} \\ \ddot{c} \end{bmatrix} = \begin{bmatrix} \boldsymbol{f}_q(t, \boldsymbol{q}, \dot{\boldsymbol{q}}, c, \dot{c}) \\ \boldsymbol{f}_c(c, \dot{c}) \end{bmatrix} + \begin{bmatrix} \boldsymbol{g}_q(t, \boldsymbol{q}, \dot{\boldsymbol{q}}) \\ \boldsymbol{g}_c(c, \dot{c}) \end{bmatrix} \begin{bmatrix} \Delta \boldsymbol{u} \\ u_c \end{bmatrix} \tag{28}$$

that, by defining $\boldsymbol{\xi} = [\boldsymbol{q}^T \ \dot{\boldsymbol{q}}^T \ c \ \dot{c}]^T$, can be rewritten as

$$\dot{\boldsymbol{\xi}} = \boldsymbol{f}(\boldsymbol{\xi}) + \boldsymbol{g}(\boldsymbol{\xi}) \begin{bmatrix} \Delta \boldsymbol{u} \\ u_c \end{bmatrix} \tag{29}$$

which is in the same form as in (11). At this point, the following constraint optimization problem is defined

$$\min_{\Delta \boldsymbol{u}, u_c} \frac{\delta_1}{2} (\Delta \boldsymbol{u} - \boldsymbol{u}_n)^T (\Delta \boldsymbol{u} - \boldsymbol{u}_n) + \frac{\delta_2}{2} (u_c - u_{c,n})^2 \tag{30}$$

$$s.t. \quad \bar{F} \geq \bar{F}_{min} \tag{31}$$

$$0 \leq \dot{c} \leq 1 \tag{32}$$

$$\boldsymbol{q}_{i,m} \leq \boldsymbol{q}_i \leq \boldsymbol{q}_{i,M}, \forall i \tag{33}$$

$$\dot{\boldsymbol{q}}_{i,m} \leq \dot{\boldsymbol{q}}_i \leq \dot{\boldsymbol{q}}_{i,M}, \forall i \tag{34}$$

$$\ddot{\boldsymbol{q}}_{i,m} \leq \ddot{\boldsymbol{q}}_i \leq \ddot{\boldsymbol{q}}_{i,M}, \forall i \tag{35}$$

$$\Delta \boldsymbol{u} \in \mathcal{N}(\boldsymbol{J}(\boldsymbol{q})) \tag{36}$$

with δ_1, δ_2 positive scalar weights. Each constraint is detailed in the following: *i)* eq. (31) handles human-multi-robot safety according to Problem 1; *ii)* eq. (32) defines the bounds for the scaling parameter $\dot{c}$. Indeed, according to the task trajectory parametrization in Sec. III-B, the parameter c plays the role of time variable t and is properly scaled to guarantee human safety. Therefore, $\dot{c} \geq 0$ means that time parameter c never decreases, meaning that the task trajectory cannot be traveled backwards. Similarly, $\dot{c} \leq 1$ means that the same trajectory cannot be traveled at a speed greater than the nominal one; *iii)* eqs. (33)-(35) take into account robots kinematic and dynamic limits in (5); *iv)* eq. (36) allows to exploit the possible redundancy of the system. Indeed, by constraining $\Delta \boldsymbol{u}$ to belong to the null-space of Jacobian $\boldsymbol{J}(\boldsymbol{q})$, the cooperative task would not be affected by this input that could be exploited to achieve additional local or global tasks encoded by $\boldsymbol{u}_n$. Each of the constraints can be handled in the framework of Exponential CBF in Section IV.

Concerning the objective function (30), it aims at finding inputs $\Delta \boldsymbol{u}$, u_c closest to $\boldsymbol{u}_n$ and $u_{c,n}$, respectively, while meeting the constraints above. The input $u_{c,n}$ is chosen as

$$u_{c,n} = k_{c,d} \, (1 - \dot{c}(t)) \tag{37}$$

with $k_{c,d} \in \mathbb{R}$ a positive gain; in view of (27), having u_c equal to $u_{c,n}$ implies $\ddot{c} = k_{c,d} \, (1 - \dot{c}(t))$ which has as asymptotic value $\dot{c} = 1$, i.e., nominal speed of the cooperative task.

VI. Simulation results

The approach presented above has been corroborated via simulations on the setup shown in Figure 1. A video can be found at the following link[2]. The setup comprises 3 cooperative robots ($N = 3$) composed of a Comau Smart Six (6-DOFs) robot mounted on a mobile base (2-DOFs). For each robot, it holds $p = 6$, $n_i = 8$ ($i = 1, 2, 3$) and the following kinematic and dynamic bounds are considered: $\boldsymbol{q}_{i,m} = \left[-30, -30, -2.97, -3, -1.57, -3.7, -2.27, -44\right]^T$, $\boldsymbol{q}_{i,M} = \left[30, 30, 2.97, 1.13, 1.4, 3.7, 2.27, 50\right]^T$ (first two components are m, others are rad); $\dot{\boldsymbol{q}}_{i,m} = \left[2, 2, 2.4, 2.8, 3, 7.85, 6.5, 9.5\right]^T$, $\dot{\boldsymbol{q}}_{i,M} = -\dot{\boldsymbol{q}}_{i,m}$ (first two components are m/s, others are rad/s); $\boldsymbol{\tau}_{i,M} = \left[500, 500, 877, 1460, 558, 46, 58, 46\right]^T$, $\boldsymbol{\tau}_{i,m} = -\boldsymbol{\tau}_{i,M}$ (first two components are m/s^2, others are rad/s^2).

Robots perform cooperative load transportation tasks between two picking stations (PS1 and PS2 in Figure 1) and a depositing one (DS), while a human operator first reaches base station BS1 and, then, moves from BS1 to BS2. To achieve the robotic task, $\boldsymbol{\sigma}(\boldsymbol{x})$ in (6) is expressed

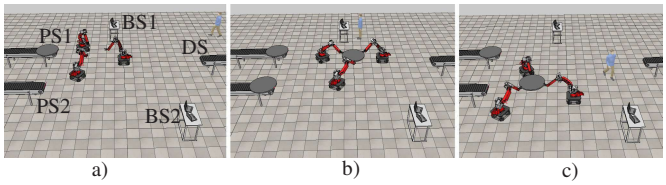

Fig. 1. Snapshots of the key phases of the simulation: Figure (a) reports the initial configuration of the work-cell; Figures (b) and (c) show the first and the second cooperative transport motions, respectively. Picking (PSi, $i = 1, 2$) and depositing (DS) stations are highlighted as well as the two base stations of the human operator (BSi, $i = 1, 2$).

by specifying both position and orientation of the centroid of the end effector poses and their relative configuration as in [13]. The absolute variables $\boldsymbol{\sigma}_1 \in \mathbb{R}^p$ are obtained as

$$\boldsymbol{\sigma}_1 = \frac{1}{N} \sum_{i=1}^{N} \boldsymbol{x}_i = \boldsymbol{J}_{\sigma_1} \boldsymbol{x} \tag{38}$$

with $\boldsymbol{J}_{\sigma_1} = \frac{1}{N} \boldsymbol{1}_N^T \otimes \boldsymbol{I}_p \in \mathbb{R}^{p \times Np}$; instead, the relative variables, denoted by $\boldsymbol{\sigma}_2 \in \mathbb{R}^{(N-1)p}$, are expressed as

$$\boldsymbol{\sigma}_2 = [(\boldsymbol{x}_N - \boldsymbol{x}_{N-1})^T \dots (\boldsymbol{x}_2 - \boldsymbol{x}_1)^T]^T = \boldsymbol{J}_{\sigma_2} \boldsymbol{x} \tag{39}$$

from which the expression of $\boldsymbol{J}_{\sigma_2} \in \mathbb{R}^{(N-1)p \times Np}$ can be derived. By stacking together absolute and relative variables in (38) and (39), respectively, the task function in (6) is $\boldsymbol{\sigma} = \boldsymbol{J}_\sigma \boldsymbol{x}$ with $\boldsymbol{J}_\sigma = [\boldsymbol{J}_{\sigma_1}^T \ \boldsymbol{J}_{\sigma_2}^T]^T \in \mathbb{R}^{m \times m}$ and $m = Np$. As foreseen by the approach and formally stated in Problem 1, a nominal desired trajectory $\boldsymbol{\sigma}_n(t)$ is planned for $\boldsymbol{\sigma}$.

Functions α_1, α_2, m in (14) are chosen as in (15) with $m_h = 0.1$ m/s, $f_{min} = 0.1$, while $k_{\sigma,d}$ and $k_{\sigma,p}$ in (10) are set to 20 and 100, respectively, and $k_{c,d} = 4$ in (37); moreover, $n_o = 15$ is considered in (18) to take into account significant human points like head, neck, torso, shoulders, arms [16]. Finally, $\bar{F}_{min}(t)$ in Problem 1 is chosen constant and equal to 33, while $\delta_1 = \delta_2 = 1$ are set in (30).

In Figure 2, the value of $\bar{F}(t)$ is reported. The blue line represents the safety field, while the green one is in correspondence of $\bar{F}_{min}$. The figure shows that the field is saturated to the minimum value in two different phases, that are when the human operator is reaching BS1 (Figure 1(b), between $t \approx 12$ s and $t \approx 17$ s) and robots are cooperatively moving from PS1 to DS, and when the human is crossing the workspace while robots are moving from PS2 to DS (Figure 1(c), between $t \approx 50$ s and $t \approx 53$ s).

Figure 3 shows the scaling parameters $c(t)$, $\dot{c}(t)$, $\ddot{c}(t)$ (in blue) compared to the nominal values t, $\dot{t} = 1$, $\ddot{t} = 0$

[2]http://webuser.unicas.it/lai/robotica/video/HMRIMED2021.mp4

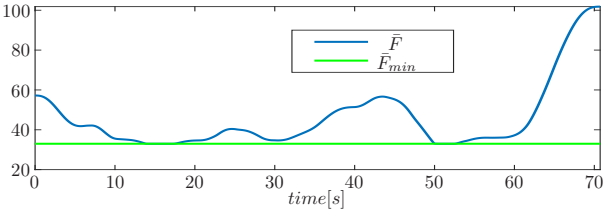

Fig. 2. Safety field evolution. The blue line represents $\bar{F}(t)$ while the green one corresponds to $\bar{F}_{min} = 33$.

(in green), respectively. A slowing down of the trajectory ($\dot{c}(t) < 1$) occurs in correspondence of the field saturation phases mentioned above in order to guarantee human safety. Other scaling phases are due to the requirement of meeting accelerations bounds as shown in the following. Note that, by virtue of (37), the condition $\dot{c} = 1$ is restored after the scaling phases, i.e., the nominal trajectory is restored. Finally, Figure 4 shows how the CBF-based approach can

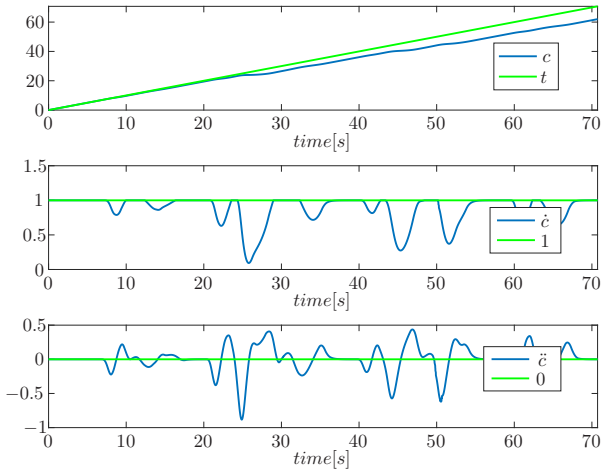

Fig. 3. Scaling parameters. The blue lines represent scaling parameters while the green ones correspond to nominal values.

handle multiple constraints. In detail, the figure reports the time plots of the first two components of $\ddot{\boldsymbol{q}}_i$ ($i = 1, 2, 3$), denoted by $\ddot{q}_{i,j}$ with $j = 1, 2$, (the only ones subject to saturation in this case study) and the corresponding bounds (in green). Figure shows how bounds are rigorously met. The other components are not shown for the sake of brevity.

VII. Conclusions

In this paper, we proposed a trajectory scaling approach for guaranteeing human safety in multi-robot settings. We first defined a safety field to assess the human level of safety with respect to the entire team of robots. Then, we set up an optimization problem based on CBF formulation to guarantee a minimum level of human safety as well as to ensure that kinematics and dynamics constraints of the robots are fulfilled. As future work, we aim to perform experiments on a real setup and to include human prediction techniques to increase the system proactivity.

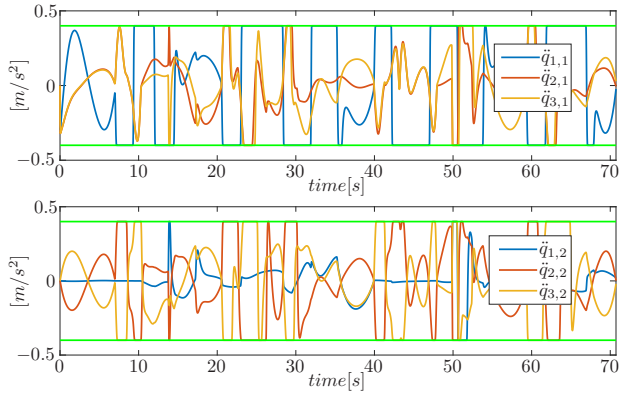

Fig. 4. Joint accelerations. The top and bottom plots show first and second components, respectively, of $\ddot{\boldsymbol{q}}_i$ for $i = 1, 2, 3$ (in blue) and minimum and maximum allowed values (in green).

References

[1] S. Robla-Gómez, V. M. Becerra, J. R. Llata, E. González-Sarabia, C. Torre-Ferrero, and J. Pérez-Oria, "Working together: A review on safe human-robot collaboration in industrial environments," *IEEE Access*, vol. 5, pp. 26 754–26 773, 2017.

[2] M. Lippi and A. Marino, "Human multi-robot safe interaction: A trajectory scaling approach based on safety assessment," *IEEE Trans. Control Syst. Technol.*, pp. 1–16, 2020.

[3] M. Safeea, P. Neto, and R. Bearee, "On-line collision avoidance for collaborative robot manipulators by adjusting off-line generated paths: An industrial use case," *Rob. Auton. Syst.*, vol. 119, pp. 278–288, 2019.

[4] A. Mohammed, B. Schmidt, and L. Wang, "Active collision avoidance for human–robot collaboration driven by vision sensors," *Int. J. Computer Integr. Manuf.*, vol. 30, no. 9, pp. 970–980, 2017.

[5] B. Lacevic, P. Rocco, and A. M. Zanchettin, "Safety assessment and control of robotic manipulators using danger field," *IEEE Trans. Robot.*, vol. 29, no. 5, pp. 1257–1270, 2013.

[6] E. Magrini, F. Ferraguti, A. J. Ronga, F. Pini, A. De Luca, and F. Leali, "Human-robot coexistence and interaction in open industrial cells," *Robot. Computer Integr. Manuf.*, vol. 61, p. 101846, 2020.

[7] M. Faroni, M. Beschi, and N. Pedrocchi, "An MPC framework for online motion planning in human-robot collaborative tasks," in *IEEE Int. Conf. Emerging Technol. Factory Autom.*, 2019, pp. 1555–1558.

[8] F. Ferraguti, M. Bertuletti, C. T. Landi, M. Bonfè, C. Fantuzzi, and C. Secchi, "A control barrier function approach for maximizing performance while fulfilling to ISO/TS 15066 regulations," *IEEE Robot. Autom. Lett.*, vol. 5, no. 4, pp. 5921–5928, 2020.

[9] A. M. Zanchettin, N. M. Ceriani, P. Rocco, H. Ding, and B. Matthias, "Safety in human-robot collaborative manufacturing environments: Metrics and control," *IEEE Trans. Autom. Sci. Eng.*, vol. 13, no. 2, pp. 882–893, 2016.

[10] A. Dahlin and Y. Karayiannidis, "Adaptive trajectory generation under velocity constraints using dynamical movement primitives," *IEEE Control Syst. Lett.*, vol. 4, no. 2, pp. 438–443, 2020.

[11] A. Bajcsy, S. L. Herbert, D. Fridovich-Keil, J. F. Fisac, S. Deglurkar, A. D. Dragan, and C. J. Tomlin, "A scalable framework for real-time multi-robot, multi-human collision avoidance," in *IEEE Int. Conf. Robot. Autom.*, 2019, pp. 936–943.

[12] D. Claes and K. Tuyls, "Multi robot collision avoidance in a shared workspace," *Autonomous Robots*, vol. 42, no. 8, pp. 1749–1770, 2018.

[13] F. Basile, F. Caccavale, P. Chiacchio, J. Coppola, and A. Marino, "A decentralized kinematic control architecture for collaborative and cooperative multi-arm systems," *Mechatronics*, vol. 23, no. 8, pp. 1100–1112, 2013.

[14] B. Siciliano, "A closed-loop inverse kinematic scheme for on-line joint-based robot control," *Robotica*, vol. 8, no. 3, p. 231–243, 1990.

[15] E. A. Basso and K. Y. Pettersen, "Task-priority control of redundant robotic systems using control lyapunov and control barrier function based quadratic programs," 2020.

[16] M. Ye, Q. Zhang, L. Wang, J. Zhu, R. Yang, and J. Gall, *A Survey on Human Motion Analysis from Depth Data*. Berlin, Heidelberg: Springer Berlin Heidelberg, 2013, pp. 149–187.

[17] U. R. Acharya, K. P. Joseph, N. Kannathal, C. M. Lim, and J. S. Suri, "Heart rate variability: a review," *Medical and Biological Engineering and Computing*, vol. 44, no. 12, pp. 1031–1051, 2006.